Structure and Magnetism of MnGa Ultra-Thin Films on GaAs(111)B

A. W. Arins, H. F. Jurca, J. Zarpellon, J. Varalda, I. L. Graff, W. H. Schreiner, and D. H. Mosca

Laboratório de Superfícies e Interfaces, Universidade Federal do Paraná, Curitiba PR 81531-990 Brazil

MnGa alloys with compositions in the range of 52 to 60 at. % Mn were grown by molecular beam epitaxy (MBE) on GaAs(111)B substrates. High quality epilayers were obtained at growth temperatures between 25 and 250°C. Epilayers are stabilized by post-growth annealing at 400°C for 30 min. *In situ* reflection high energy electron diffraction (RHEED) and X-ray photoelectron spectroscopy (XPS) have been performed to probe surface structure and stoichiometry during growth and post-annealing process. *Ex situ* X-ray diffraction (XRD) measurements were also performed in order to access the bulk crystalline structure using synchrotron radiation source. MnGa epilayers are formed by stacking of (111) planes of tetragonal zinc-blende structure (ZB) which are rotated by approximately 11° with respect to the underlying (111) planes of the GaAs lattice. The tetragonal ZB structure of MnGa exhibits lattice parameters of $a = 0.55$ nm and $c = 0.61$ nm. Magnetic measurements performed using a vibrating sample magnetometer (VSM) reveal nearly isotropic in-plane magnetization with saturation magnetization varying between 650 and 300 emu/cm^3 for different concentrations of Mn.

Index Terms—**Epitaxial films, magnetic hysteresis, MnGa alloys, saturation magnetization.**

I. Introduction

Bulk binary alloys of $\mathrm{Mn_xGa_{1-x}}$ $(50\% \leq x \leq 75\%)$ exhibit a wide range of saturation magnetization and magnetic anisotropy values with Curie temperatures above room temperature. The complex phase diagram of Mn-Ga system whose framework was established fifty years ago [1]–[4] also exhibit a variety of crystalline phases.

In films, a variety of MnGa nanocrystalline structures have been formed by controlling the Mn/Ga ratio and the substrate temperature during growth by MBE. MnGa alloys grown on GaAs semiconductors by MBE are particularly interesting candidates for applications in spintronics as spin injectors due to their thermodynamic stability, large spin polarization, square-like hysteresis loops, and large magnetic anisotropy [5]–[11]. Several phases and compounds are found for different growth conditions [12]–[17]. Mn-Ga alloys films with composition range 62–76 at. % Mn are commonly found in the tetragonal δ-phase, adopting both $\mathrm{D0_{22}}$- and $\mathrm{L1_0}$-type structures [16]. Their Curie temperatures are above room temperature and magnetic moments as high as 2.5 μ_B per unit cell have been reported [5], [18]. Electrical spin injection from δ-MnGa into a Ga(Al)As-based light-emitting diode was already demonstrated at remanence, i.e., without an applied magnetic field [19]. Therefore, these compounds are attractive for use in spin-valves, magnetic tunnel junction devices operating under perpendicular magnetic anisotropy, and spin injectors into semiconductors.

Based on the success of epitaxial grown MnGa on GaN [15], we investigate in this work the growth and magnetic properties of MnGa films overgrown on treated epi-ready GaAs(111)B substrates. Once the growth completed, these films are subsequently annealed *in situ*. During the growth of the MnGa alloy films its surface structure was monitored by RHEED, whereas the bulk crystalline structure was investigated by XRD (*ex situ*). The face-centered tetragonal (fct) δ-MnGa with CuAu-$\mathrm{L1_0}$-type ordering proposed by Niida *et al.* [16] for bulk and powder samples was not observed for ultrathin films. In addition, other crystalline phase is observed from XRD analyses. The vibrating sample magnetometry measurements have revealed ferromagnetic behavior with smaller in-plane magnetic anisotropy. All films thicker than 20 nm exhibit polycrystalline character independently of the film stoichiometry (between 40 and 63 at. % Mn) and annealing procedure.

II. Experiment

The MnGa layers were grown by solid-source MBE on insulating GaAs(111)B epiready wafers in a custom-designed ultrahigh vacuum MBE system, equipped with Ga and Mn effusion cells whose fluxes were measured using a residual gas analyzer. *In situ* growth was monitored by real-time RHEED and surface stoichiometry was determined by XPS, performed using a VG Microtech ESCA3000 spectrometer installed in an in tandem chamber equipped with a conventional Mg/Al X-ray source which has an overall resolution of 0.8 eV at a 45° emission angle.

Prior to MnGa growth, removal of the oxide layer of epiready GaAs(111)B wafers at 580°C was performed with a subsequent Ga pre-exposure. RHEED pattern of a smooth GaAs(111)B surface characterized by a (1×1) reconstruction is obtained. Several MnGa growth experiments were performed setting substrate temperatures at $\mathrm{T_s} = 25, 50, 150$ or 250°C, respectively, with an appropriate flux ratio R of Mn to Ga to achieve the particular stoichiometry in the films. According to *in situ* XPS analyses, the surface stoichiometry of the MnGa films varies from 52 to 63 at. % Mn for R ranged in between 1 and 2. Under these conditions by opening Mn and Ga shutters during 24 min, MnGa layers with thicknesses of 5 nm were obtained. Thereafter, $\mathrm{T_s}$ was ramped up to 400°C at 3°C/min in order to anneal the films during 30 min.

XPS spectra of Ga $2\mathrm{p}_{3/2}$ and Mn $2\mathrm{p}_{3/2}$ core-levels were performed *in situ* at different stages of growth and subsequently after annealing to monitor surface stoichiometry. Only the presence of $\mathrm{Ga^{2+}}$ and $\mathrm{Mn^{2+}}$ spectral components are found in the

Manuscript received February 16, 2013; revised March 28, 2013; accepted April 12, 2013. Date of current version November 20, 2013. Corresponding author: D. H. Mosca (e-mail: mosca@fisica.ufpr.br).

Color versions of one or more of the figures in this paper are available online at http://ieeexplore.ieee.org.

Digital Object Identifier 10.1109/TMAG.2013.2272213

0018-9464 © 2013 IEEE

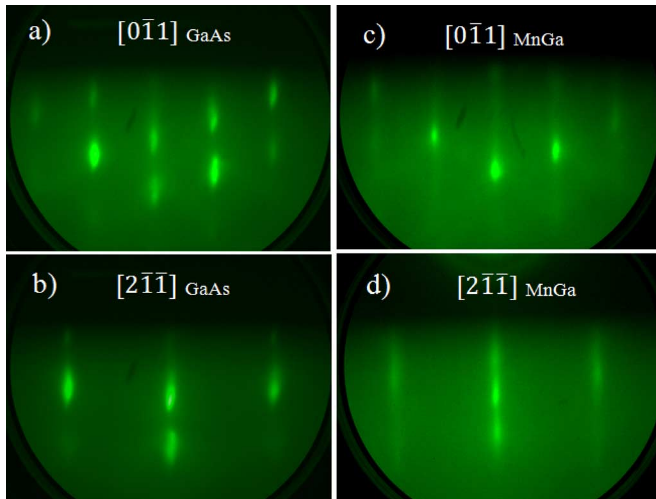

Fig. 1. RHEED patterns taken along the azimuths [0 $\bar{1}$ 1] and [2 $\bar{1}$ $\bar{1}$] of epiready GaAs(111)B substrates after removal of the oxide layer at 580° C are respectively shown in (a) and (b). RHEED patterns corresponding to the same azimuths of GaAs after MnGa layer grown on GaAs(111)B surface at 50° C for 24 min, and subsequently annealed at 400° C for 30 min, are respectively shown in (c) and (d).

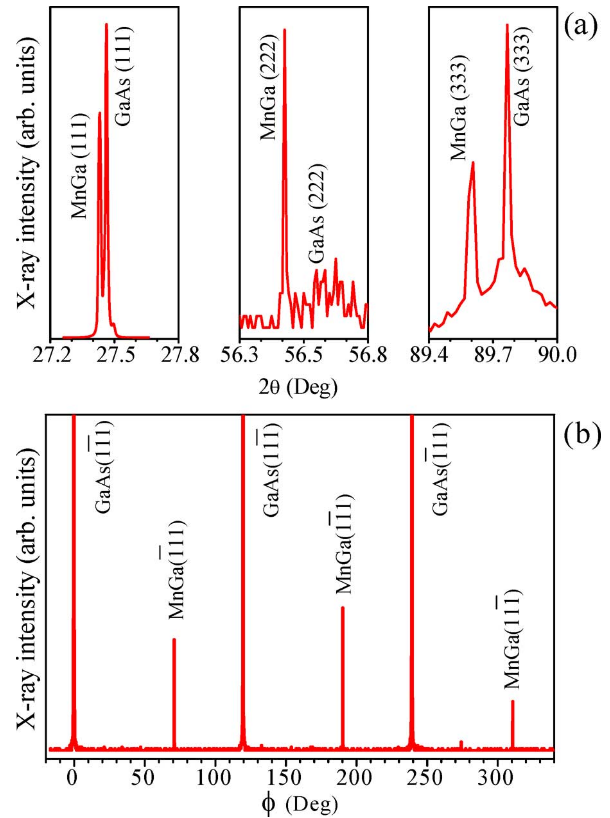

Fig. 2. (a) θ–2θ cans for MnGa epilayer grown during 24 min and (b) ϕ scan for same sample by turning the film plane around the axis (1 $\bar{1}$ 1) of the GaAs substrate, which is 70.5° off from the film normal.

XPS spectra, suggesting that Mn-Ga alloying and Ga-Ga interaction perturbed by the nearby Mn are the predominant processes under growth conditions. The exponential attenuation of As 2p photopeak does not show evidences of shift nor broadening, which is another argument to establish the presence of MnGa alloying. Based on such observations we can estimate the growth rate of the films at 0.2 nm/min.

III. Results and Discussion

RHEED patterns measured along the respective [0 $\bar{1}$ 1] and [2 $\bar{1}$ $\bar{1}$] azimuths of the (1×1)-reconstructed surface of GaAs (111)B, as stabilized after removal of the oxide layer at 580 oC, are shown in Fig. 1(a) and (b). Even the removal of the oxide layer being conducted without an As flux to control the surface As concentration, it was observed that only a GaAs(111)B-(1×1) reconstruction was present, known as the $(1 \times 1)_{\mathrm{HT}}$ phase [16], [17]. RHEED patterns obtained from the MnGa layer with flux ratio $\mathrm{R} = 1$ cooled down to 50°C after annealing are shown in Fig. 1(c) and (d). These RHEED patterns indicate high quality epitaxy of the MnGa layer with in-plane interplanar spacings quite similar to those of GaAs. The in-plane symmetry of MnGa layer is equivalent to that of GaAs(111)B surface. However, sharper RHEED patterns are systematically found shifted by approximately 11° off the angular positions corresponding to the [0 $\bar{1}$ 1] and [2 $\bar{1}$ $\bar{1}$] azimuths of GaAs. The in-plane interatomic distances of MnGa are respectively 0.343 and 0.201 nm along the [0 $\bar{1}$ 1] and [2 $\bar{1}$ $\bar{1}$] azimuths of GaAs.

Ex situ XRD experiments were performed using a conventional x-ray diffractometer at the Brazilian synchrotron source (LNLS). θ–2θ scans are shown in Fig. 2(a). Bragg peak corresponding to (111) interplanar spacing of GaAs centered at $2\theta = 27.4°$ exhibit a concurrent Bragg peak assigned to (111) plane of MnGa with $\mathrm{d}(111) = 0.327$ nm. Similar features are observed at larger angles for (222) and (333) Bragg peaks. The pseudo-forbidden condition for GaAs(222) peak due to similar atomic factors between Ga and As is less effective in the case of Ga and Mn. The epitaxy of MnGa on GaAs(111) is confirmed by a ϕ scan shown in Fig. 2(b). This ϕ scan was obtained by turning the sample around an axis 70.5° off the [111] axis of the GaAs substrate in order to evidence the diffraction peaks of the {$\bar{1}$ 1 1} family planes. The Bragg diffraction peaks corresponding to GaAs(1 $\bar{1}$ 1) planes are observed spaced by 120°. Diffraction peaks assigned to MnGa layer are also spaced by 120°, but rotated by 71° (or 49°) with respect to the diffraction peaks of GaAs. XRD and RHEED results are therefore consistent with an epitaxial relationship given by GaAs(111) // MnGa (111) in the normal direction to the surface of the films and with each plane $(0\ \bar{1}\ 1)$ and $(2\ \bar{1}\ \bar{1})$ of MnGa rotated by 11° with respect to the planes $(0\ \bar{1}\ 1)$ and $(2\ \bar{1}\ \bar{1})$ of GaAs. These findings are consistent with a tetragonal ZB cell with $c = 0.61$ nm and $a = 0.55$ nm instead of a body-centered cubic tetragonal (bct) cell for MnGa with lattice parameters $a' = 0.28$ nm and $c' = 0.31$ nm, as previously reported [5], [6]. It is worth of note that a bct cell can be derived from two juxtaposed face-centered tetragonal (fct) cells of MnGa preserving the geometrical rules of a stable $\mathrm{L1}_o$-type structure [16].

Therefore, RHEED and XRD analyses are consistent with MnGa layer adopting tetragonal ZB cell with $c = 0.61$ nm and $a = 0.55$ nm [20]. Such tetragonal ZB cell can be formed by assuming $c \approx 2c'$ and $a \approx 2a'$, which results from the stacking of bct(111) planes onto GaAs(111)B-(1×1) reconstructed surface. The rotation angles 49° and 71° between MnGa and GaAs

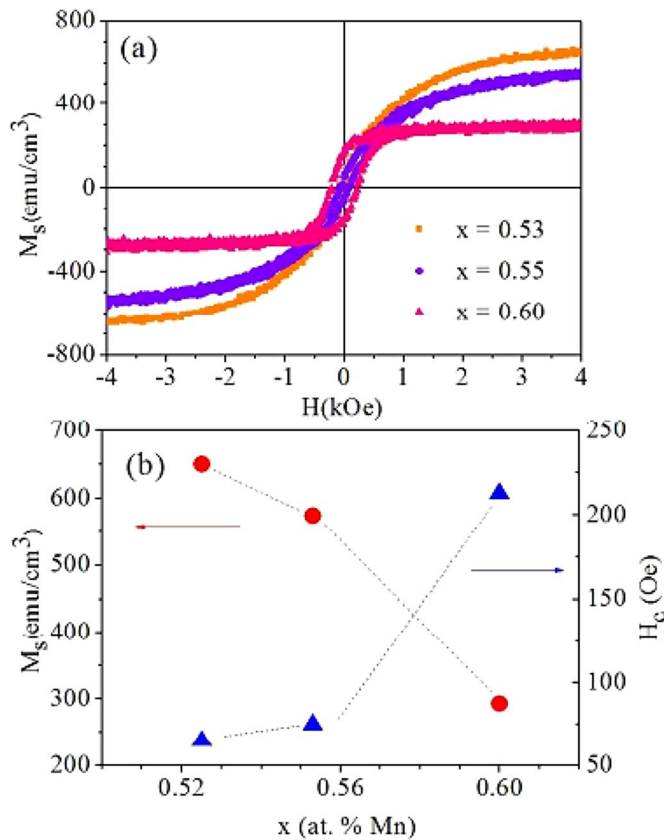

Fig. 3. (a) Magnetic hysteresis loops measured at room temperature and (b) saturation magnetization and coercivity as a function of the composition for 5-nm-thick $Mn_{1-x}Ga_x$/GaAs(111) epilayers.

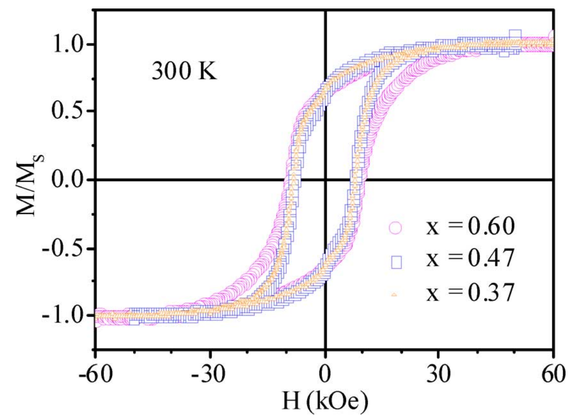

Fig. 4. Magnetic hysteresis loops measured at room temperature of 100-nm-thick polycrystalline $Mn_{1-x}Ga_x$/GaAs(111) films. The magnetic field was applied in plane along [110] direction.

lattices shown in Fig. 2(b) can be obtained by a tetragonal distortion of about ~2% in the ZB cell and rotation by 11° of MnGa lattice with respect to GaAs. These features are confirmed by RHEED analyses shown in Fig. 1. Tetragonal ZB structure occurs for film thicknesses not exceeding 20 nm. Independent of the Mn content, thicker films of MnGa are (111)-textured even if annealed during longer time. It is indicating that tetragonal ZB phase is found only for ultrathin MnGa films.

Magnetic properties of ultrathin MnGa films epitaxially grown on GaAs(111)B can be inferred from the Fig. 3(a) and (b). Hysteresis loops were measured using a vibrating sample magnetometer (PPMS Evercool II—Quantum Design) at room temperature with magnetic fields applied out of the film plane and parallel to projections of c and a crystallographic axis in the film plane.

According to Fig. 3(a) saturation magnetization value as high as $\mathrm{MS} = 650$ emu/cm^3, which corresponds to 12.9 μ_B per tetragonal ZB cell or 3.2 μ_B per Mn atom, can be found for $x = 0.53$ (53 at·% Mn). Tetragonal ZB MnGa films exhibit nearly isotropic in-plane magnetization [20]. It suggests the possibility to exist equivalent epitaxial domains rotated by 120° one relative to the other, which could reduce the anisotropy along a and c crystallographic axes. However, since MnGa epilayers have a tetragonal distortion with $c/a = 1.11$, magnetoelastic anisotropy contributions cannot be disregarded. Fig. 3(b) shows a trend of decrease in the saturation magnetization and increase in the coercivity when Mn content goes from 0.5 to 0.6 in these ultrathin films with tetragonal ZB structure.

The room-temperature saturation magnetization and the coercive field change markedly with alloy composition. As already reported by Bedoya-Pinto *et al.* [12], the saturation magnetization M_s and coercive field H_C show opposite trends. In fact, in Mn_xGa_{1-x} epitaxial layers with $L1_o$ structure the magnetic behavior depends not only on the alloy composition, it is also sensitive to lattice strain since the incorporation of additional Mn atoms simultaneously alters the strain state. These two effects have been treated independently in theoretical studies. According to Sakuma *et al.* [21], the excess Mn atoms in MnGa alloys with $L1_o$ structure will have an antiparallel alignment to the rest, leading to a decrease of the magnetic moment. In another theoretical work, Yang *et al.* [22] calculated the strain dedencence in stoichiometric MnGa, showing that the reduction of the lattice parameter leads to a smaller magnetic moment. Although the effect of the Mn incorporation and the induced strain cannot be separated in our films, which exhibit a tetragonal zinc-blend structure, the decrease of the magnetic moment with increasing Mn concentration is in qualitative agreement with the trends predicted by these works.

In Fig. 4 are shown the hysteresis loops measured at room temperature for thicker Mn-Ga films which are polycrystalline with (111)-texture; i.e., where the (111) planes are preferentially orientated along the normal of the film plane. These films containing from 30 to 60 at. % Mn have thickness of about 100 nm and saturation magnetization values of about 475 emu/cm^3. Despite the saturation magnetization values smaller those observed for very thin films, their coercivities are nonetheless much higher, with values as large as 8–9 kOe. These films are therefore interesting to the development of nanoscale hard magnets. The H_C increase with Mn concentration in films is probably related to local strain variations and chemical disorder due to additional Mn incorporation. Thicker films can also exhibit different phases with the development of secondary preferential orientations. Large H_c is possibly linked to the presence of the disordered $L1_o$ phase and $DO_{22}Mn_3Ga$ phase [23]. Another possible contributions to the H_C changes should be imperfection of the films including chemical disorder, lattice defects and strains. Particularly, the probability of correct site occupation in the crystal structure often has significant

influence on the magnetic properties of the $L1_O$-ordered alloy films [24].

IV. Conclusion

MnGa films with tetragonal zinc-blend structure were directly grown on GaAs(111) substrates. Films with thicknesses greater than 20 nm are polycrystalline exhibiting a crystalline texture with (111) planes preferentially oriented parallel to the film plane. The magnetic behavior and structure of the equi-stoichiometric MnGa ultrathin films with tetragonal zinc-blend structure are unstable, exhibiting significant decrease of saturation magnetization values and increase of the coercivity by increasing either Mn content or thicknesses.

Our present results reveal an interesting approach to explore and control magnetic behavior in these alloys which are suitable for spintronic applications.

Acknowledgment

The authors thank Fabiano Yokaichiya (LNLS, Campinas) for support and help during the XRD measurements. This work was supported in part by the CNPq, Fundação Araucária (Grant PRONEX 17386 #118/2010), and Brazilian Synchrotron Light Laboratory (LNLS) under proposal XPD-12533. H. F. J. thanks CAPES/PRODOC and J. Z. thanks REUNI/UFPR. This paper was presented at the X Latin American Workshop On Magnetism, Magnetic Materials And Their Applications (X-LAW3M 2013) (*IEEE Trans. Magn.*, vol. 49, no 8, pt. 1, Aug. 2013).

References

[1] I. Tsuboya and M. Sugihara, *J. Phys. Soc. Jpn.*, vol. 18, p. 143, 1963.
[2] M. Hasegawa and I. Tsuboya, *J. Phys. Soc. Jpn.*, vol. 20, p. 464, 1965.
[3] H.-G. Meißner, K. Schubert, and Z. Metallkd, vol. 56, p. 523, 1965.
[4] T. A. Bither and W. H. Cloud, *J. Appl. Phys.*, vol. 36, p. 1501, 1965.
[5] M. Tanaka *et al., Appl. Phys. Lett.*, vol. 62, p. 1565, 1993.
[6] M. Tanaka, *Mater. Sci. Eng. B*, vol. 31, p. 117, 1995.
[7] W. Van Roy, H. Akinaga, S. Miyanishi, and K. Tanaka, *Appl. Phys. Lett.*, vol. 69, p. 711, 1996.
[8] W. Van Roy, H. Akinaga, and S. Miyanishi, *Phys. Rev. B*, vol. 63, p. 184417, 2001.
[9] K. M. Krishnan, *Appl. Phys. Lett.*, vol. 61, p. 2365, 1992.
[10] W. Feng *et al., J. Appl. Phys.*, vol. 108, p. 113903, 2010.
[11] Z. Bai *et al., Appl. Phys. Lett.*, vol. 100, p. 022408, 2012.
[12] A. Bedoya-Pinto *et al., Phys. Rev. B*, vol. 84, p. 104424, 2011.
[13] T. A. Bither and W. H. Cloud, *J. Appl. Phys.*, vol. 36, p. 1501, 1965.
[14] F. Wu *et al., Appl. Phys. Lett.*, vol. 94, p. 122503, 2009.
[15] E. Lu *et al., Phys. Rev. Lett.*, vol. 97, p. 146101, 2006.
[16] H. Niida *et al., J. Appl. Phys.*, vol. 79, p. 5946, 1996.
[17] H. Kurt *et al., Phys. Rev. B.*, vol. 83, p. 020405, 2011.
[18] Z. Yang *et al., J. Magn. Magn. Mater.*, vol. 182, p. 369, 1998.
[19] C. Adelmann *et al., App. Phys. Lett.*, vol. 89, p. 112511, 2006.
[20] A. W. Arins, H. F. Jurca, J. Zarpellon, J. Varalda, I. L. Graff, A. J. A. de Oliveira, W. H. Schreiner, and D. H. Mosca, *Appl. Phys. Lett.*, vol. 102, p. 102408, 2013.
[21] A. Sakuma, *J. Magn. Magn. Mater.*, vol. 187, p. 105, 1998.
[22] Z. Yang, J. Li, D. Wang, K. Zhang, and X. Xie, *J. Magn. Magn. Mater.*, vol. 182, p. 369, 1998.
[23] C. L. Zha, R. K. Dumas, J. W. Lau, S. M. Mohseni, S. R. Sani, I. V. Golosovsky, A. F. Monsen, J. Nogue's, and J. Akerman, *J. Appl. Phys.*, vol. 110, p. 093902, 2011.
[24] L. Zhu, S. Nie, K. Meng, D. Pan, J. Zhao, and H. Zheng, *Adv. Mater.*, vol. 24, p. 4547, 2012.